Research Article

Guo Zhang, Haiyang Zhu, Qi Wang, Xiaowen Zhang, Mingfa Ren*, Shunan Xue and Gang Li

Buckling analysis of thin-walled metal liner of cylindrical composite overwrapped pressure vessels with depressions after autofrettage processing

https://doi.org/10.1515/secm-2021-0051
received May 08, 2021; accepted September 02, 2021

Abstract: The cylindrical filament wound composite overwrapped pressure vessels (COPV) with metal liner has been widely used in spaceflight due to their high strength and low weight. After the autofrettage process, the plastic deformation of the metal liner is constrained by composite winding layers, which introduce depressions to the metal liner that causes local buckling. To predict the local buckling of the inner liner with depressions of the pressure vessel after the autofrettage process, a local buckling analysis method for the metal liner of COPV was developed in this article. The finite element method is used to calculate the overall stress distribution in the pressure vessel before and after the autofrettage process, and the influence of local depressions on the buckling is evaluated. The axial buckling of the pressure vessel under external pressure is analyzed. The control equation of the metal liner with depressions is developed, considering the changes in the pressure and the bending moment of the liner depressions and its vicinity during the loading and unloading process. Taking the cylindrical COPV (38 L) with aluminum alloy liner as an example, the effects of liner thickness, liner radius, the thickness-to-diameter ratio, autofrettage pressure, and the length of straight section on the autofrettage process are discussed. The results show that the thickness of the inner liner has the most significant influence on the buckling of the liner, followed by the length of the straight section and the radius of the inner liner, while the autofrettage pressure has the least influence.

Keywords: autofrettage processing, buckling analysis, composite overwrapped pressure vessels

*** Corresponding author: Mingfa Ren,** Department of Engineering Mechanics, Dalian University of Technology, Dalian 116024, China; Department of Engineering Mechanics, The State Key Laboratory of Structural Analysis for Industrial Equipment, Dalian University of Technology, Dalian 116024, China, e-mail: renmf@dlut.edu.cn, tel: +86-411-8470-9161,
fax: +86-411-8470-9161
Guo Zhang: Department of Engineering Mechanics, Dalian University of Technology, Dalian 116024, China; Beijing Chinatank Industry Co. Ltd, Beijing 100024, China
Haiyang Zhu: Department of Engineering Mechanics, Dalian University of Technology, Dalian 116024, China; National Key Laboratory of Combustion, Thermal Structure and Flow, Xi'an Aerospace Propulsion Institute, Xi'an 710125, China
Qi Wang, Shunan Xue: Department of Engineering Mechanics, Dalian University of Technology, Dalian 116024, China
Xiaowen Zhang: School of Materials Science and Engineering, Dalian University of Technology, Dalian 116024, China
Gang Li: Department of Engineering Mechanics, Dalian University of Technology, Dalian 116024, China; Department of Engineering Mechanics, The State Key Laboratory of Structural Analysis for Industrial Equipment, Dalian University of Technology, Dalian 116024, China

1 Introduction

As a core component of the space reentry vehicle, pressure vessels occupy the largest proportion of weight and volume in the propulsion system, which is the most significant part of the carrier structures [1,2]. Due to the anisotropy, designability, lightweight, and high strength of the composite materials, the weight of composite overwrapped pressure vessels (COPV) can be reduced by about 25% compared to metal pressure vessels. Therefore, COPV have been widely applied in aerospace structures and process equipment in recent years [3–10]. COPV are mainly divided into cylindrical pressure vessels, spherical pressure vessels, annular pressure vessels by shape, of which the cylindrical pressure vessels are most widely used for their advantages of simple structure and high filling coefficient [11]. By the type of structure, the cylindrical COPV can be divided into circumferentially wound COPV with metal liner, metal liner COPV,

liner-less COPV, and so on. To make full use of the high strength of composites and the plasticity of the metal material [12], the wound layer should bear most of the load under the working pressure, while the inner liner only acts as a seal. Therefore, the thin-walled liner structure is adopted, and the autofrettage process that exceeds its working pressure is applied to the pressure vessel before it is put into use [13,14]. Then, after the autofrettage pressure is completely unloaded, the residual compressive stresses remain in the metal liner. Under working pressure, this pre-stressed state can make the stress distribution COPV more reasonable, effectively reduce the stress level of the liner [15–19] and significantly improve the overall capacity of COPV [20–23].

After the autofrettage process of the COPV, the plastic state of the metal liner is under compression. Therefore the liner is prone to buckling deformation, which will greatly reduce the load-bearing capacity and service life of the COPV [24]. Aggarwal and Cooper [25] conducted 49 sets of experiments to study the liner buckling under different boundary conditions. The results indicate that, for the same inner liner, when the outer side is rigidly restrained, the critical buckling load is 7 times larger than that of the unconstrained one. Yang et al. [26] developed a 3D finite element analysis (FEA) of the COPV by equating the wound layer to composite laminates. With the FEA method, the nonlinear buckling analysis of the COPV with metal liner was carried out, and the multiphase buckling modes and critical buckling loads were obtained. Fu et al. [27] used the FEA of nonlinear buckling analysis to obtain the buckling mode shapes of the cylinder liner. At the same time, the relationship between the liner displacement and the external pressure was established, and the critical buckling external pressure of the inner liner was obtained. Liang et al. [28] used the eigenvalue analysis method to calculate the critical buckling pressure of the cylinder liner of COPV. It is found that the critical bucking pressure becomes more sensitive to the geometric depression by increasing the length-to-diameter ratio. The buckling of the metal liner of COPV is solved as a global buckling problem under external pressure in these studies. Therefore, the finite element model of the eigenvalue analysis or nonlinear analysis is established to study the stability of the metal liner after the autofrettage process.

However, the buckling deformation of the COPV liner after the autofrettage process is the unilateral buckling constrained by the outer wound layer, which is generally expressed as the local buckling of the metal liner. Hu et al. [29] used acoustic emission technology to study the buckling deformation of the liner of COPV in the unloading process of internal pressure and found that the deformation between the composite layers and the liner was incompatible, which resulted in the buckling deformation and the failure of the liner. High-amplitude acoustic signals were detected in the unloading process, and local buckling of the liner due to the release of stress waves from structural buckling was observed. The results suggest that the local buckling will generate in the unloading of the autofrettage process rather than the global buckling.

In addition, from the perspective of the manufacturing process of COPV, foreign objects may be mixed during the winding process and the inner liner may be hit by hard objects occasionally. These factors induce initial depressions into the inner liner, which will further increase the possibility of local buckling around the depressions [30]. This kind of depressions can be avoided through strict production management. However, during the autofrettage process of the filament wound thin-walled metal-lined COPV, at the overlap of the first layer and the second layer of the fiber tape, due to the uneven distribution, the matrix material will be compacted to increase the rigidity under the action of autofrettage pressure, which will inevitably cause the thin-walled metal liner to produce a certain depth of depression after the autofrettage processing [31]. In view of the research on the local buckling problem of the COPV liner with depressions, based on the assumption of plane strain, scholars simplified the cylindrical inner liner into a cylindrical ring, carried out an analysis of the circumferential buckling of the cylindrical ring with depression. Zhou [32] carried out external pressure buckling tests on thin-walled stainless steel liners and obtained the critical buckling loads of different sizes of liners. Lo et al. [33] equated the buckling part of the ring to a rod with initial curvature and used the elliptic integral function to derive the post-buckling topography. Sun et al. [34] conducted research on the shrinkage buckling of the inner liner through theoretical derivation and experimental research and found that the buckling load is very sensitive to the small depressions of the rigid boundary. Based on the theory of finite deflection, Yamamoto and Matsubara [35,36] studied the buckling of the cylindrical ring under external pressure and found that the initial depression can decrease the critical buckling pressure of the cylindrical ring. Based on the finite element method (FEM), Wang et al. [37] established a simplified ring model of the ultra-thin metal liner of COPV with depressions on the liner and realized the numerical simulation of the local buckling of the liner. With the nonlinear FEM, Vasilikis [38,39] established the 2D model to conduct the numerical simulation of the cylinder and its surrounding medium. The results showed that the critical buckling pressure is sensitive to the initial buckling depression.

The cylindrical COPV's liner is simplified to be a cylindrical ring for buckling analysis, and the analytical and numerical solutions of critical buckling can be obtained. The influence of axial stress and deformation on buckling is neglected. However, studies have shown that after autofrettage processes, the liner is simultaneously constrained by the winding layer in circumferential and axial directions, and the axial stress and deformation of the liner have a great influence on buckling [28]. The cylindrical pressure vessel is more likely to have axial buckling after the autofrettage process. It is also found that the liner has a damaged morphology caused by local buckling in the axial direction (as shown in Figure 1).

According to the buckling analysis on the metal line of COPV with the initial depression, Phoenix and Kezirian [31] believed that the elastic support of the composite material winding layer on the liner limits the deformation of the liner. When the axial in-plane pressure N of the liner is greater than the axial critical pressure N_{cr} of the liner, the liner will not buckle but the initial depression will cause the interface pressure between the liner and the winding layer to change. If the interface pressure is less than 0 and the length of the residual bending moment of the inner liner distributed in the axial direction is greater than the half-wavelength of the in-plane axial buckling, the liner will buckle. The buckling analysis of a metal line of spherical COPV with depression is carried out, and the problem is simplified to a square thin plate model on an elastic foundation subjected to a bidirectional load. And in the process of solving, using the symmetry of the square thin plate to further solve the elastic surface differential equation of the rectangular thin plate by the ordinary differential equation, and the analytical solution of the inner bladder interface pressure and residual bending moment is obtained. This study mainly used the equal stress and deformation of the spherical shell in all directions. It is believed that the critical buckling load of the square thin plate with side length as half the wavelength of spherical shell buckling in both directions is equal to the critical buckling load of the spherical shell. However, the stress and deformation of the cylindrical pressure vessel in the hoop and axial directions are inconsistent, which makes the listed three-dimensional elastoplastic equations unable to be simplified accordingly, and it is difficult to obtain the required analytical solutions for the in-plane tension N and the interface pressure. If a three-dimensional finite element model for the buckling analysis of

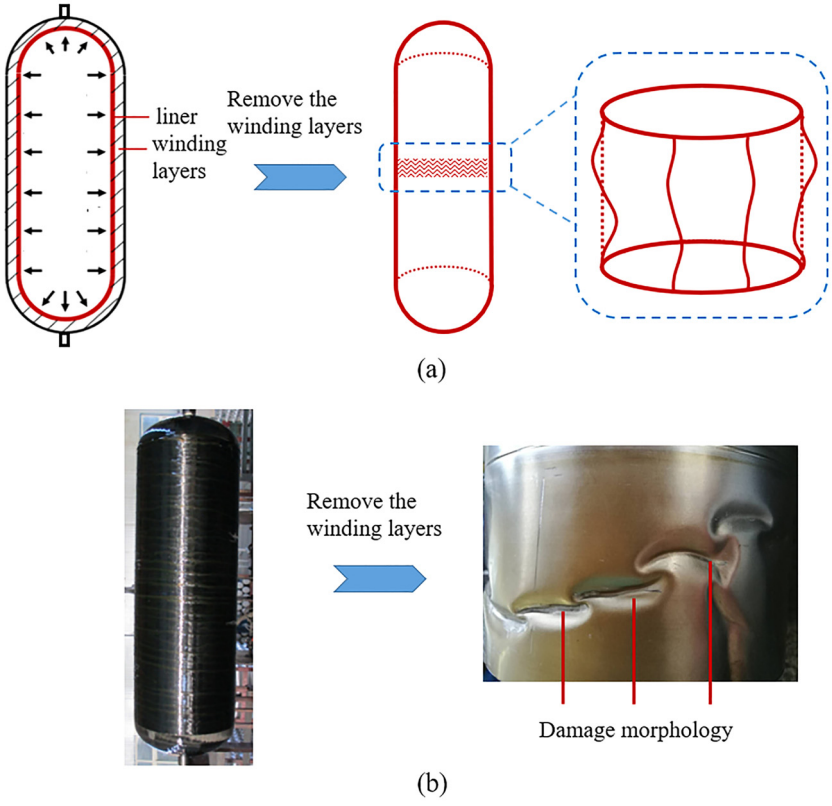

Figure 1: Damaged morphology of COPV with metal liner caused by local buckling in the axial direction. (a) Schematic diagram of the axial local buckling of the metal liner and (b) damage appearance of the metal liner resulting from axial buckling after the autofrettage process.

the inner liner with initial depressions is established for cylindrical COPV, the contact between the liner and the winding layer must be defined, and the different contact states of the depression and the winding layer before and after the autofrettage need to be considered. Meanwhile, the contact area has strict requirements on the quality and accuracy of the mesh [40], which often makes it difficult to obtain the calculation results of convergence. In addition, there is obvious stress concentration near the depression, and the liner will enter the plastic flow state earlier in the vicinity of the depression [41], resulting in an ill-conditioned stiffness matrix during the solution process, which will further cause the calculation results of the FEM not to converge, and therefore, it is impossible to obtain accurate calculation results [41,42].

In this article, a novel buckling analysis method for the metal liner of cylindrical COPV with depressions is proposed. Firstly, the stress distributions of pressure vessels before and after autofrettage are calculated by FEA to obtain the in-plane tension and interface pressure of the metal liner; Secondly, an analytical model of the effect of depression on the interface pressure and residual bending moment of the liner is established to calculate the change in the depression profile before and after the autofrettage to determine whether the metal liner will be locally buckled. Then, the effect of the changes of dimensional parameters on local buckling of cylindrical COPV with initial depressions is further discussed, such as the autofrettage pressure, liner thickness, radius, and thickness-to-diameter ratio.

2 Establishment of the analysis method

2.1 Buckling criterion of metal liners with depression

For the thin-walled liner of cylindrical COPV, the straight section is a cylindrical shell. Under the pressure of the autofrettage process, the liner will be plastically deformed, and the composite winding layer is always in an elastic state [22]. After the pressure is unloaded, the liner will be in a compressed state. The critical buckling pressure F_{Ncr} of the cylindrical shell under the axial load is [42]

$$F_{\mathrm{Ncr}} = \frac{E_{\mathrm{l}} t_{\mathrm{l}}^2}{R_{\mathrm{l}} \sqrt{3(1-\mu^2)}}, \tag{1}$$

where E_{l} is the elastic modulus of liners, t_{l} is the thickness of liners, R_{l} is the radius of liners, and μ is the Poisson ratio of the liners.

The buckling wavelength λ corresponding to the critical in-plane buckling pressure of a cylindrical shell under pressure is [42]

$$\lambda = 2m\pi \left(\frac{R_{\mathrm{l}}^2 t_{\mathrm{l}}^2}{12(1-\mu^2)} \right)^{\frac{1}{4}}, \tag{2}$$

where m is the order. Taking $m = 1$ and dividing the wavelength by 2, the half-wavelength of the buckling is obtained as

$$\frac{\lambda}{2} = \pi \left(\frac{R_{\mathrm{l}}^2 t_{\mathrm{l}}^2}{12(1-\mu^2)} \right)^{\frac{1}{4}}. \tag{3}$$

The distance between the zero points of the residual bending moment of the liners near the depressions is greater than $\pi(R_{\mathrm{l}}^2 t_{\mathrm{l}}^2/12(1-\mu^2))^{1/4}$. The interface pressure between the liner and the winding layer is less than 0. If the above three conditions are met at the same time, local buckling of the liner occurs.

2.2 Overall calculation process

The metal liners of the cylindrical COPV usually thicken the sealing section and the transition regions from the straight section to the sealing section under the spinning process, and the middle part of the straight section is the thinnest. This results in the straight section being more likely to produce an initial depression under the autofrettage pressure and the local buckling after unloading [22]; so, the metal liner in the straight section with initial depressions is studied in this article.

The commercial software ANSYS is utilized for the simulation calculation of the FEM. A geometrical model of the 1/8 cross-section of the cylindrical COPV with metal liner is established, where the type of SOLID 46 element is employed for the metal liner and type of SOLID 45 element is employed for composite layers. The contact elements CONTA174 are added between the metal liner and the composite layers for the calculations of the stress distribution of the liner before and after autofrettage pressure. The symmetrical boundary conditions are carried out by the edges of the FEM. The axial stress of each node in the middle of the straight section of the FEM is extracted along with the thickness orientation of the liner, and integrated with the thickness direction to obtain the in-plane pressure of the thin-walled metal liner.

With the deduction, an analytical model was established for the contour changes of the straight cylinder section with depressions before and after the autofrettage process, and the analytical model of the effect of the depression on the liner interface pressure and residual bending moment.

If the deformation distribution of the cylindrical shell in the axial and circumferential directions is considered at the same time, a partial differential equation system needs to be established, which cannot be resolved. Therefore, only the displacement distribution in one direction is considered, the ordinary differential equation is listed, and the influence of the other direction is corrected in the equation to solve it. Brush [43] has used a simply supported beam model on the elastic foundation to describe the deformation of the cylindrical shell under confining pressure. The specific method was to extract the beam model along the axial direction of the cylindrical shell to obtain the displacement distribution of the cylindrical shell along the axis. Since the beam model is in one dimension, in order to describe the influence of the circumferential stiffness, the displacement of the beam restricted by the circumferential direction of the cylindrical shell is taken as equivalent to the stiffness treatment of the elastic foundation.

In this way, when analyzing the change of displacement along the axial direction of the cylindrical shell, the two-dimensional problem is simplified to a one-dimensional problem, and the partial differential equation is simplified into the ordinary differential equation as follows [43]

$$D\frac{\mathrm{d}^4w}{\mathrm{d}x^4} - F_\mathrm{N}\frac{\mathrm{d}^2w}{\mathrm{d}x^2} + \left(\frac{E_\mathrm{l}t_\mathrm{l}}{R_\mathrm{l}^2}\right)w = 0, \tag{4}$$

where w is the radial displacement of the liner, N_l is the axial in-plane tension of the liner, F_N is the axial in-plane tension of the liner, D is the lateral stiffness of the liner, E_l is the elastic modulus of the liner, t_l is the thickness of the liner, μ_l is the Poisson ratio, and R_l is the radius of the liner.

In the middle of the cylindrical shell, assuming the initial depth of the depression is δ, then the coordinates of the center position of the depression are taken as $w(x = 0) = \delta$. The boundary condition of the equation is defined as $\lim_{|x|\to\infty}w(x) = 0$, $\lim_{|x|\to 0}\mathrm{d}w(x)/\mathrm{d}x = 0$, in combination with the boundary condition, the above ordinary differential equation can be solved to obtain the radial direction of the cylindrical shell. Then, the derivative of the equation is taken to obtain the shear force and the bending moment. In addition, for the cylindrical COPV, the influence of the lateral stiffness of the outer winding layers on the deformation of the inner liners should be taken into account. Therefore, the lateral stiffness correction term should be added to the linear term of the governing equation (the stiffness term of the elastic foundation) to reflect this effect, and obtain the governing equation,

$$D\frac{\mathrm{d}^4w}{\mathrm{d}x^4} - F_\mathrm{N}\frac{\mathrm{d}^2w}{\mathrm{d}x^2} + \left(\frac{E_\mathrm{l}t_\mathrm{l}}{R_\mathrm{l}^2}+\frac{E_\mathrm{O}}{t_\mathrm{O}}\right)w = 0. \tag{5}$$

Considering the change of the in-plane tension of the pressure vessel before and after the autofrettage process and the contour change of the depression on the surface of the cylindrical shell in the autofrettage process, equation (5) is solved. The interface pressure and residual bending moment of the metal liner at the depression can be obtained. The calculation flow chart is shown in Figure 2.

2.3 Solution of depression profile, interface pressure, the and residual bending moment

2.3.1 Establishment of the control equation on the depression profile

In order to facilitate the solution of the governing equation (5), dimensionless processing is performed to obtain

$$\frac{\mathrm{d}^4w(x)}{\mathrm{d}x^4} - 2F_\mathrm{l}\cdot\frac{\mathrm{d}^2w(x)}{\mathrm{d}x^2} + \Phi\cdot w(x) = 0, \tag{6}$$

where

$$F_l = \frac{6F_\mathrm{N}(1-\mu_\mathrm{l}{}^2)}{E_\mathrm{l}t_\mathrm{l}^3}, \tag{7}$$

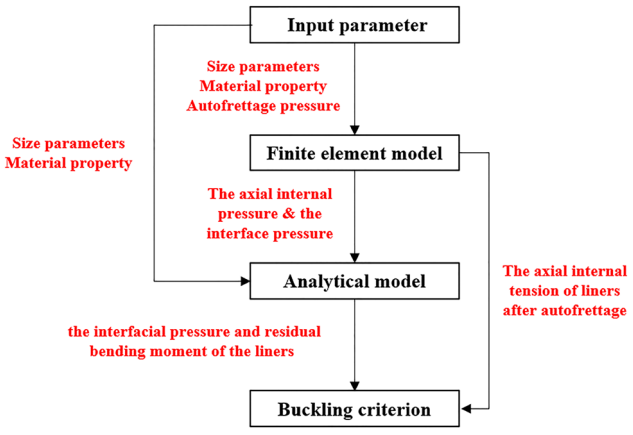

Figure 2: Calculation flow chart.

$$\Phi_1 = \left(\frac{E_l t_l}{R_l^2} + \frac{E_O}{t_o}\right) \Big/ \left(\frac{E_l t_l^3}{12(1-\mu_l^2)}\right). \tag{8}$$

Here, $E_{O,t}$ is the elastic modulus of the winding layer, t_O is the thickness of the winding layer, R_l is the radius of the inner liner, and p_{in} is the autofrettage pressure.

In order to obtain the interface pressure and the residual bending moment of the inner liner depression during the loading phase, the ordinary differential equation (6) is transformed: $F_{l1} = \frac{6F_{N1}(1-\mu_l^2)}{E_l t_l^3}$, where F_{N1} is the axial in-plane tension of the liner when the autofrettage pressure reaches its peak, $\Phi_1 = \left(\frac{E_l t_l}{R_l^2} + \frac{E_O}{t_o}\right) \Big/ \left(\frac{E_l t_l^3}{12(1-\mu_l^2)}\right)$. The transverse stiffness of the winding layer is the same as that before compaction and it is 1/10 of the transverse rigidity after compaction.

Define the initial depth of the depression δ_b and the boundary conditions $w_1(x=0) = -\delta_{b1}$, $\lim_{|x|\to\infty} w_1(x) = 0$, $\lim_{|x|\to 0} \frac{dw_1(x)}{dx} = 0$, the solution of the equation can be obtained:

$$w_1(x) = -\delta_{b1} e^{-\omega_1 \varphi_1 \cdot |x|} [\varphi_1 \cdot \sin(\omega_1 \cdot |x|) + \cos(\omega_1 \cdot x)], \tag{9}$$

where the values of each parameter are $\omega_1 = \sqrt[4]{\Phi_1} \cdot \sqrt{\frac{\sqrt{\Phi_1} - F_{l1}}{2\sqrt{\Phi_1}}}$ and $\varphi_1 = \sqrt[4]{\Phi_1} \cdot \sqrt{\frac{\sqrt{\Phi_1} + F_{l1}}{\sqrt{\Phi_1} - F_{l1}}}$.

Taking the derivative of the solution 4 times, and substituting it into the governing equation (6), and sorting out the governing equation with the initial depression profile,

$$\begin{aligned} &\frac{d^4 w_1(x)}{dx^4} - 2F_{l1} \cdot \frac{d^2 w_1(x)}{dx^2} + \Phi_1 \cdot w_1(x) \\ &\quad + 4\omega_1^3 \cdot (1 + \varphi_1^2) \cdot \varphi_1 \cdot \delta_{b1} \cdot \delta(x) = 0. \end{aligned} \tag{10}$$

The fourth derivative is

$$\begin{aligned} \frac{d^4 w_1(x)}{dx^4} &= \Phi_1 \cdot \delta_{b1} \cdot e^{-\omega_1 \varphi_1 \cdot |x|} \cdot [\varphi_1 \cdot \sin(\omega_1 \cdot |x|) \\ &\quad + \cos(\omega_1 \cdot x)] - 4\omega_1^3 \cdot (1 + \varphi_1^2) \cdot \varphi_1 \cdot \delta_{b1} \cdot \delta(x) \\ &\quad + 2\omega_1^4 \cdot (1 + \varphi_1^2) \cdot (-1 + \varphi_1^2) \cdot \delta_{b1} \cdot e^{-\omega_1 \varphi_1 \cdot |x|} \\ &\quad \cdot [-\varphi_1 \cdot \sin(\omega_1 \cdot |x|) + \cos(\omega_1 \cdot x)]. \end{aligned} \tag{11}$$

From the first two terms of equitation (11), the expression of the interface pressure is obtained as

$$\begin{aligned} p_l(x) &= C \cdot E_l I_l \cdot \omega_1^4 \cdot (1 + \varphi_1^2)^2 \cdot \delta_{b1} \cdot e^{-\omega_1 \varphi_1 \cdot |x|} \\ &\quad \cdot [\varphi_1 \cdot \sin(\omega_1 \cdot |x|) + \cos(\omega_1 \cdot x)] \\ &\quad - 4C \cdot E_l I_l \cdot \omega_1^3 \cdot (1 + \varphi_1^2) \cdot \varphi_1 \cdot \delta(x), \end{aligned} \tag{12}$$

where C is the coefficient of the residual bending moment, and the bending stiffness $E_l I_l$ of the liner is

$$E_l I_l = \frac{E_l t_l^3}{12(1-\mu_l^2)}. \tag{13}$$

The expression $p_p(x)$ for the local pressure distribution at the center of the depression is [31]

$$\begin{aligned} p_p(x) &= \frac{F_{pc} \cdot (1 + \varphi_1^2) \cdot \omega_1}{4\varphi_1} \cdot e^{-\omega_1 \varphi_1 \cdot |x|} \cdot [\varphi_1 \cdot \sin(\omega_1 \cdot |x|) \\ &\quad + \cos(\omega_1 \cdot x)] - F_{pc} \cdot \delta(x), \end{aligned} \tag{14}$$

where

$$F_{pc}(x) = -4C \cdot E_l I_l \cdot \omega_1^3 \cdot (1 + \varphi_1^2) \cdot \varphi_1. \tag{15}$$

As equation (14) involves the function δ, it is not easy to understand their effects intuitively. Therefore, the line load $F_{pc} \cdot \delta(x)$ in the region is processed with interpolation, which does not affect the overall analysis of the change in the depression profile [31]. Assuming that

$$p_{pc}(x) = -p_{max} \cdot \left[A \cdot \left(\frac{x}{x_c}\right)^4 - B \cdot \left(\frac{x}{x_c}\right)^2 + 1\right], \tag{16}$$

where $-x_c < x < x_c$. To ensure the continuity of the solution, the boundary condition is defined as the value and the sloppiness of the pressure distribution at the transition line, $x = x_c$, are 0, and then the two undetermined coefficients of the above equation can be determined.

$$p_{pc}(x) = -p_{max} \cdot \left[\left(\frac{x}{x_c}\right)^4 - 2\left(\frac{x}{x_c}\right)^2 + 1\right]. \tag{17}$$

In order to show the equivalent effect, the integral of the interface pressure in the dispersion region is equal before and after the numerical processing [31], and it can be determined as

$$p_{max} = \frac{15F_{pc}}{16x_c}. \tag{18}$$

The dispersed local interface pressure can be expressed as

$$p_{pc}(x) = \begin{cases} \left[\left(\frac{x}{x_c}\right)^4 - 2\left(\frac{x}{x_c}\right)^2 + 1\right] \cdot \left(-\frac{15F_{pc}}{16x_c}\right), & -x_c < x < x_c \\ 0, & x < -x_c \ \text{or} \ x > x_c, \end{cases} \tag{19}$$

The analytical solution of the interfacial pressure of the whole field is

$$p_1(x) = \begin{cases} \dfrac{F_{pc}\cdot(1+\varphi_1^2)\cdot\omega_1}{4\varphi_1}\cdot e^{-\omega_1\varphi_1\cdot|x|}\cdot[\varphi_1\cdot\ \sin(\omega_1\cdot|x|)+\ \cos(\omega_1\cdot x)]+p_{pc}, & -x_c < x < x_c \\ \dfrac{F_{pc}\cdot(1+\varphi_1^2)\cdot\omega_1}{4\varphi_1}\cdot e^{-\omega_1\varphi_1\cdot|x|}\cdot[\varphi_1\cdot\ \sin(\omega_1\cdot|x|)+\ \cos(\omega_1\cdot x)], & x > x_c \text{ or } x < -x_c. \end{cases} \tag{20}$$

The distribution of the bending moments is

$$M_p(x) = \begin{cases} \dfrac{F_{pc}}{4\omega_1\varphi_1}\cdot[\cos(\omega_1\cdot x)-\varphi_1\cdot\ \sin(\omega_1\cdot|x|)]\cdot e^{-\omega_1\varphi_1\cdot|x|}+\Theta, & -x_c < x < x_c \\ \dfrac{F_{pc}}{4\omega_1\varphi_1}\cdot[\cos(\omega_1\cdot x)-\varphi_1\cdot\ \sin(\omega_1\cdot|x|)]\cdot e^{-\omega_1\varphi_1\cdot|x|}, & x > x_c \text{ or } x < -x_c, \end{cases} \tag{21}$$

where

$$\Theta = F_{pc}\cdot x_c\cdot\left[\frac{1}{32}\left(\frac{x_c^6-x^6}{x_c^6}\right)-\frac{5}{32}\left(\frac{x_c^4-x^4}{x_c^4}\right)+\frac{15}{32}\left(\frac{x_c^2-x^2}{x_c^2}\right)-\frac{1}{2}\left(\frac{x_c-|x|}{x_c}\right)\right]. \tag{22}$$

Substituting $x = 0$, the residual bending moment distribution at the center of the depression can be obtained as

$$M_p(0)=\frac{F_{pc}}{4\omega_1\varphi_1}-\frac{5}{32}F_{pc}\cdot x_c. \tag{23}$$

If $M_p(0) = M_{pf,max}$, where $M_{pf,max}$ is the maximum plastic moment, we can obtain

$$x_c = \frac{8}{5\omega_1\varphi_1}-\frac{32M_{pf,\ max}}{5F_{pc}}. \tag{24}$$

2.3.2 Deformation analysis of depression in the unloading stage

Starting from the governing equation (6) for the depression profile, the displacement solution of the initial depression profile is defined as

$$w_1(x) = -\delta_{b,0}\cdot e^{-\omega_1\varphi_1\cdot|x|}[\varphi_1\cdot\ \sin(\omega_1\cdot|x|)+\ \cos(\omega_1\cdot x)]. \tag{25}$$

Define the lateral displacement in the unloading stage w_f as the sum of the displacement increment (caused by the axial load F_N applied at each phase) and the initial displacement of the liner depression, then

$$w_f(x) = w(x) - w_1(x). \tag{26}$$

In the unloading stage, the lateral displacement of the lining differential equation shall meet the following equitation:

$$\frac{d^4w_f(x)}{dx^4}-2F_l\cdot\frac{d^2w(x)}{dx^2}+\Phi_2\cdot w_f(x)=0. \tag{27}$$

In the second term on the left of the equation, the applied load depends on the total displacement and so w is the total displacement.

The general solution of the inhomogeneous equation (28) is

$$w_f(x) = e^{-\omega_1\varphi_1\cdot x}\cdot[A\cdot\ \sin(\omega_1\cdot x)+B\cdot\ \cos(\omega_1\cdot x)], \tag{28}$$

where A and B are undetermined coefficients, which can be obtained by using the method of undefined coefficient:

$$A=\frac{H+I}{F+G},\quad B=\frac{J+K}{F+G}, \tag{29}$$

where

$$\begin{aligned} F &= [(\omega_1\cdot\varphi_1)^4-6(\omega_1\cdot\varphi_1)^2\cdot{\omega_1}^2+{\omega_1}^4-2F_l\cdot(\omega_1\cdot\varphi_1)^2+2F_l\cdot\omega_1^2+\Phi_2]^2 \\ G &= [-4\cdot(\omega_1\cdot\varphi_1)^3\cdot\omega_1+4\cdot(\omega_1\cdot\varphi_1)\cdot{\omega_1}^3+4F_l\cdot(\omega_1\cdot\varphi_1)\cdot\omega_1]^2 \\ H &= -[(\omega_1\cdot\varphi_1)^4-6(\omega_1\cdot\varphi_1)^2\cdot{\omega_1}^2+{\omega_1}^4-2F_l\cdot(\omega_1\cdot\varphi_1)^2+2F_l\cdot\omega_1^2+\Phi_2]\cdot\varphi_1 \\ I &= -4\cdot(\omega_1\cdot\varphi_1)^3\cdot\omega_1+4\cdot(\omega_1\cdot\varphi_1)\cdot{\omega_1}^3+4F_l\cdot(\omega_1\cdot\varphi_1)\cdot\omega_1 \\ J &= [4(\omega_1\cdot\varphi_1)^3\cdot\omega_1-4(\omega_1\cdot\varphi_1)\cdot{\omega_1}^3-4F_l(\omega_1\cdot\varphi_1)\cdot\omega_1]\cdot\varphi_1 \\ K &= (\omega_1\cdot\varphi_1)^4-6(\omega_1\cdot\varphi_1)^2\cdot{\omega_1}^2+{\omega_1}^4-2F_l\cdot(\omega_1\cdot\varphi_1)^2+2F_l\cdot\omega_1^2+\Phi_2, \end{aligned} \tag{30}$$

in which $\omega_1 = \sqrt[4]{\Phi_1} \cdot \sqrt{\frac{\sqrt{\Phi_1} - F_{l1}}{2\sqrt{\Phi_1}}}$, $\varphi_1 = \sqrt[4]{\Phi_1} \cdot \sqrt{\frac{\sqrt{\Phi_1} + F_{l1}}{\sqrt{\Phi_1} - F_{l1}}}$, $\Phi_1 = \left(\frac{E_l t_l}{R_l^2} + \frac{E_O}{t_o}\right) \Big/ \left(\frac{E_l t_l^3}{12(1-\mu_l^2)}\right)$, $\Phi_2 = \left(\frac{E_l t_l}{R_l^2} + \frac{E_{O1}}{t_o}\right) \Big/ \left(\frac{E_l t_l^3}{12(1-\mu_l^2)}\right)$.

Within the interval $x > 0$, the general solution of the inhomogeneous equation is the general solution of the homogeneous equation plus a special solution of the inhomogeneous equation:

$$\begin{aligned} w_f(x) = {} & P \cdot e^{-\omega_2\varphi_2 \cdot x} \cdot \sin(\omega_2 \cdot x) + Q \cdot e^{-\omega_2\varphi_2 \cdot x} \\ & \cdot \cos(\omega_2 \cdot x) + R \cdot e^{-\omega_2\varphi_2 \cdot x} \cdot \sin(\omega_2 \cdot x) \\ & + S \cdot e^{-\omega_2\varphi_2 \cdot x} \cdot \cos(\omega_2 \cdot x) \\ & + e^{-\omega_1\varphi_1 \cdot x}[A \cdot \sin(\omega_1 \cdot x) + B \cdot \cos(\omega_1 \cdot x)]. \end{aligned} \tag{31}$$

Substituting the boundary conditions $\lim_{x\to\infty} w_f(x) = 0$, we obtain

$$R = S = 0, \tag{32}$$

$$w_f(x) = w(x) - w_1(x), \tag{33}$$

displacement w_f obtained by formula (36) is the total radial displacement of the liner during the unloading process, which is w_{f2}.

The ultimate form of moment distribution, pressure distribution, and displacement near the depression after unloading is obtained [31] as

$$M_{\text{un}}(x) = C \cdot E_l I_l \cdot \left(\frac{\mathrm{d}^2 w_{f2}}{\mathrm{d}x^2} - \frac{\mathrm{d}^2 w_{f1}}{\mathrm{d}x^2}\right), \tag{38}$$

$$p_{\text{un}}(x) = C \cdot E_l I_l \cdot E_O \cdot (1 - \mu_l^2) \cdot (w_{f2} - w_{f1})/t_O. \tag{39}$$

The specific calculation process is shown in Figure 3. In detail, an FE model is established for the COPV with a metal liner, the autofrettage pressure is applied, the in-plane tension when the autofrettage pressure reaches the peak is calculated, and the internal tension and interface pressure after the autofrettage pressure are completely unloaded. Establishing the governing equation of the

$$P = \frac{\omega_1 \cdot (B\omega_2^2\varphi_2^2\varphi_1 - B\omega_1^2\varphi_1^3 - A\omega_2^2\varphi_2^2 + 3A\omega_1^2\varphi_1^2 - 3B\omega_2^2\varphi_1 + 3B\omega_1^2\varphi_1 + 3A\omega_2^2 - A\omega_1^2)}{-2\omega_2^3(\varphi_2^2 + 1)}, \tag{34}$$

$$Q = \frac{\omega_1 \cdot (3B\omega_2^2\varphi_2^2\varphi_1 - B\omega_1^2\varphi_1^3 - 3A\omega_2^2\varphi_2^2 + 3A\omega_1^2\varphi_1^2 - B\omega_2^2\varphi_1 + 3B\omega_1^2\varphi_1 + A\omega_2^2 - A\omega_1^2)}{-2\omega_2^3\varphi_2(\varphi_2^2 + 1)}, \tag{35}$$

where $\omega_1 = \sqrt[4]{\Phi_1} \cdot \sqrt{\frac{\sqrt{\Phi_1} - F_{l1}}{2\sqrt{\Phi_1}}}$, $\varphi_1 = \sqrt[4]{\Phi_1} \cdot \sqrt{\frac{\sqrt{\Phi_1} + F_{l1}}{\sqrt{\Phi_1} - F_{l1}}}$, $\Phi_1 = \left(\frac{E_l t_l}{R_l^2} + \frac{E_O}{t_o}\right) \Big/ \left(\frac{E_l t_l^3}{12(1-\mu_l^2)}\right)$, $\omega_2 = \sqrt[4]{\Phi_2} \cdot \sqrt{\frac{\sqrt{\Phi_2} - F_{l2}}{2\sqrt{\Phi_2}}}$, $\varphi_2 = \sqrt[4]{\Phi_2} \cdot \sqrt{\frac{\sqrt{\Phi_2} + F_{l2}}{\sqrt{\Phi_2} - F_{l2}}}$, $\Phi_2 = \left(\frac{E_l t_l}{R_l^2} + \frac{E_{O1}}{t_o}\right) \Big/ \left(\frac{E_l t_l^3}{12(1-\mu_l^2)}\right)$.

Expanding the solution to $-\infty < x < +\infty$, we obtain

$$\begin{aligned} w_f(x) = {} & P \cdot e^{-\omega\varphi \cdot |x|} \cdot \sin(\omega \cdot |x|) + Q \cdot e^{-\omega\varphi \cdot |x|} \\ & \cdot \cos(\omega \cdot x) + e^{-\omega_1\varphi_1 \cdot |x|}[A \cdot \sin(\omega_1 \cdot |x|) \\ & + B \cdot \cos(\omega_1 \cdot x)], \end{aligned} \tag{36}$$

$$\begin{aligned} \frac{\mathrm{d}^2 w_f(x)}{\mathrm{d}x^2} = {} & P'' \cdot e^{-\omega\varphi \cdot |x|} \cdot \sin(\omega \cdot |x|) + Q'' \cdot e^{-\omega\varphi \cdot |x|} \\ & \cdot \cos(\omega \cdot x) + e^{-\omega_1\varphi_1 \cdot |x|}[A'' \cdot \sin(\omega_1 \cdot |x|) \\ & + B'' \cdot \cos(\omega_1 \cdot x)]. \end{aligned} \tag{37}$$

When calculating the displacement of the liner loaded by the autofrettage pressure, $E_{O1} = E_O$, the value of F_{l2} is the maximum value of in-plane tension, the displacement w_f obtained by formula (36) is the total radial displacement of the liner during the loading process, which is w_{f1}. When calculating the displacement of the liner unloaded by the autofrettage pressure, $E_{O1} = 10E_O$, the value of F_{l2} is the maximum value of the in-plane pressure, and the depression profile and solving the ordinary differential equation by substituting the above coefficients, we obtain the distribution of the interface pressure and residual bending moment near the depression after the autofrettage pressure is completely unloaded. Combined with the buckling criterion, one can judge whether the depression will cause the buckling of the liner.

3 Model validation

To validate the analysis methods applied in this article, the analytical results are compared with the results of numerical examples in the literature [31]. The results are shown in Table 1, and the initial depth of the depression is set to 0.51 and 2.04 mm, respectively, to calculate the interface pressure distribution. The results are shown in Figure 3.

The calculation results in Table 1 and Figure 4 show that the deviation between the results of the critical depth of the depression in the literature and that in this article is 7.9%, and the minimum value of the interface pressure near the depression is in good agreement.

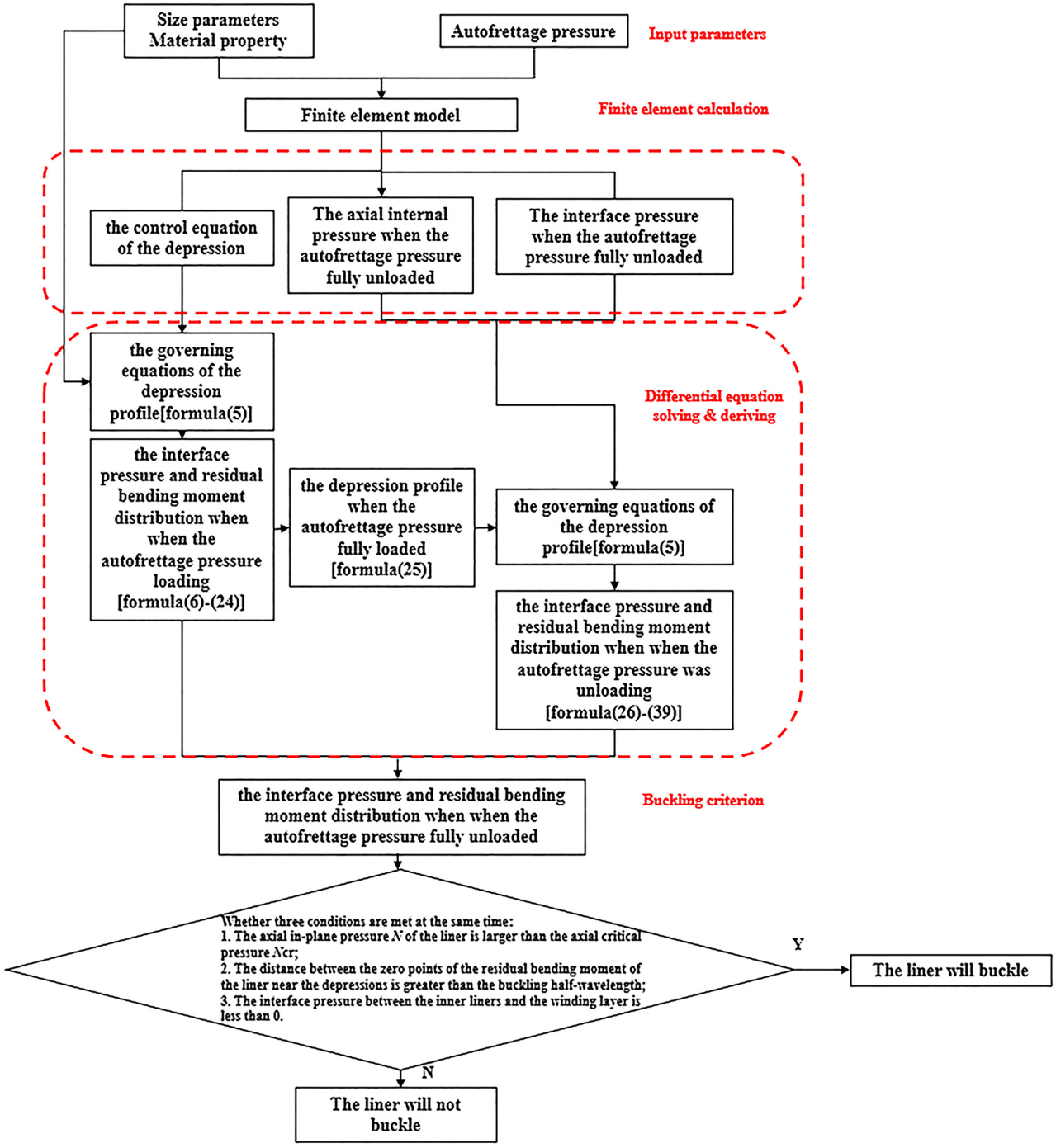

Figure 3: Calculation process.

4 Example discussion

The critical depth of the depression is defined as the minimum value of the depression depth, which is related to the autofrettage pressure, material parameters, and dimension parameters. In this article, for the cylindrical COPV with an initial depression, the calculation model for buckling analysis is established. The influence of factors such as the autofrettage pressure, the radius of the liner, the thickness of the liner, the thickness-to-diameter ratio of the liner, and the length of the straight section on the critical depth of the depression is studied.

Table 1: Comparison between the calculation results of the literature [31] and results of verification examples in this article

Item	Literature [31] results	Verification examples in this article	Deviation (%)
Material property and dimension parameter	Winding material: Kevlar 49/epoxy; Lining material: titanium alloy; Lining thickness: 2.7 mm Thickness of the winding layer: 18.8 mm Container radius: 480 mm		—
In-plane tension with full loading	2206.2 N/m	2196.5 N/m	0.4
In-plane tension with unloading completely	1491.5 N/m	1250.1 N/m	16.2
Critical depth of depression	1.65 mm	1.78 mm	7.9

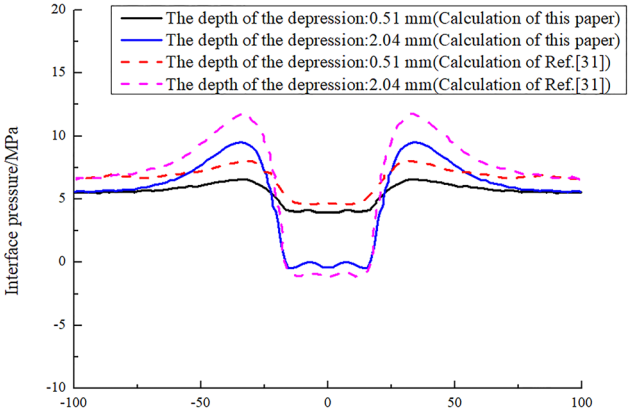

Figure 4: Comparison of interface pressure distribution calculations.

4.1 Calculation results of the interface pressure and residual bending moment

The FEM of the cylindrical COPV is established, and the cross-sectional view of the pressure vessel is shown in Figure 5. The liner of the pressure vessel is of aluminum alloy, Young's modulus is 69 GPa, the winding layer of the composite material is T700/epoxy, the length of the straight section is 270 mm, the radius of the inner liner is 170 mm, the thickness of the inner liner is 0.8 mm, and the thickness of the winding layer is 10.8 mm. The autofrettage pressure is 45 MPa. The stiffness properties of T700/epoxy are shown in Table 2.

From equation (2), the critical in-plane pressure of the liner is calculated to be 149.52 N/m. The in-plane pressure in the middle of the straight section is 192.88 N/m after autofrettage, which is larger than the critical in-plane pressure of the inner liners. Therefore, the metal liner of the example meets the first condition of the buckling criterion.

The analytical model of the metal liner of the cylindrical pressure vessel with depression was adopted for calculations. The depths of the depression are set to be 0.2, 0.4, and 0.6 mm, respectively. The change of interface pressure and residual bending moment near the depression are shown in Figure 6.

It can be seen from Figure 6 that the fluctuation range of the residual bending moment corresponding to the three depression depths is about 40 mm (the depression is about 20 mm on the left and right sides of the liner axis). From equation (3), the axial buckling half-wavelength of the liner is 20.1 mm, and the fluctuation range of the residual bending moment is larger than the axial buckling half-wavelength of the liner, which meets the second condition of the buckling criterion; When the initial depth of the depression is 0.2 mm, the interface pressure of the depression is greater than 0, which does not meet the third condition of the buckling criterion, so the initial depression with a depth of 0.2 mm will not cause local buckling of the liner. When the initial depth of the depression is 0.4 or 0.6 mm, the interface pressure has a distribution less than 0, which meets the third condition of the buckling criterion and the inner liner has the local buckling.

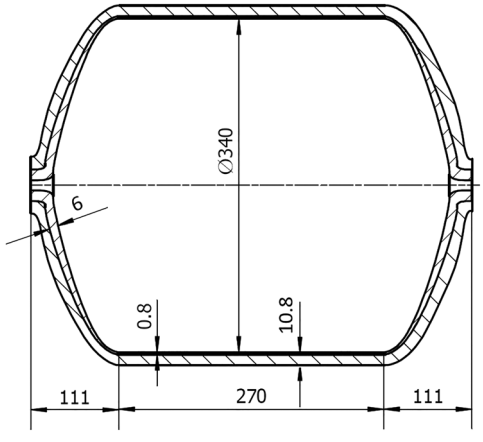

Figure 5: Section view of the pressure vessel.

Table 2: Stiffness properties of T700/epoxy

E_1 (GPa	E_2 (GPa)	E_3 (GPa)	G_{12} (GPa)	G_{13} (GPa)	G_{23} (GPa)	μ_{12}	μ_{13}	μ_{23}
150	12	12	7	5	5	0.3	0.3	0.3

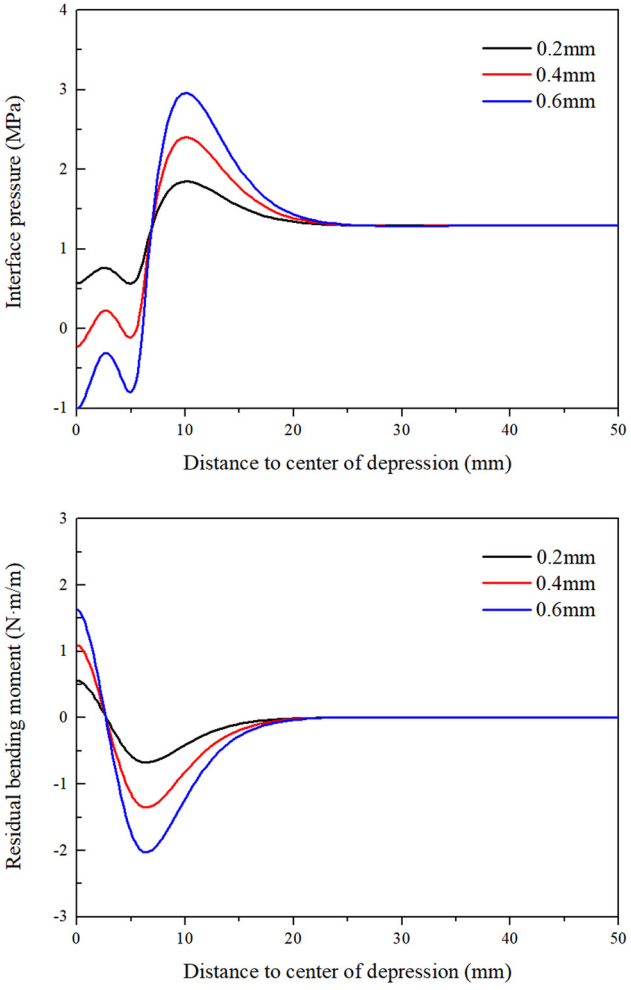

Figure 6: Distribution of (a) interface pressure and (b) residual bending moment near depressions after autofrettage.

4.2 Parameter discussion

4.2.1 Relationship between the critical depth of depression and thickness of the inner liner

Keeping the radius of the liner at 170 mm, the thicknesses of the liner are 0.7, 0.8, and 0.9 mm. The relationship between the critical depth of depression and autofrettage pressure is shown in Figure 7. The relationship between the ratio of the critical depth of the depression to the thickness of the liner (hereinafter referred to as "the depression-to-thickness ratio") and the autofrettage pressure are shown in Figure 8.

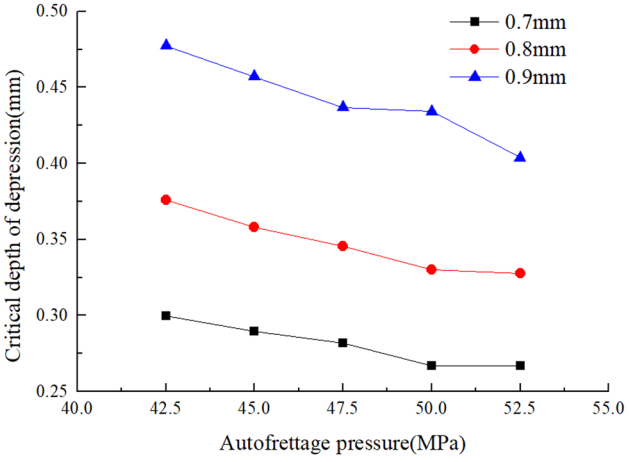

Figure 7: Relationship between the critical depth of depression and autofrettage pressure considering the variation of liner thickness.

From Figures 7 and 8, it can be seen that as the autofrettage pressure increases, the critical depth and the depression-to-thickness ratio decrease, and the critical depth level and the depression-to-thickness ratio decrease with the decrease of the liner's thickness. The critical depth corresponding to the thickness of the inner liner of 0.9 mm is significantly greater than that

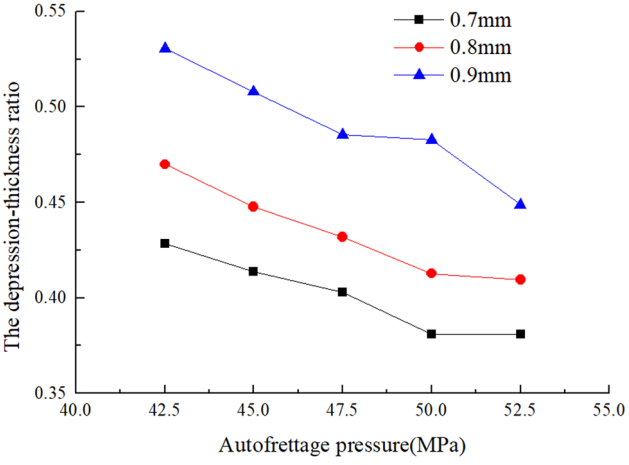

Figure 8: Relationship between the depression-thickness ratio and autofrettage pressure considering the variation of liner thickness.

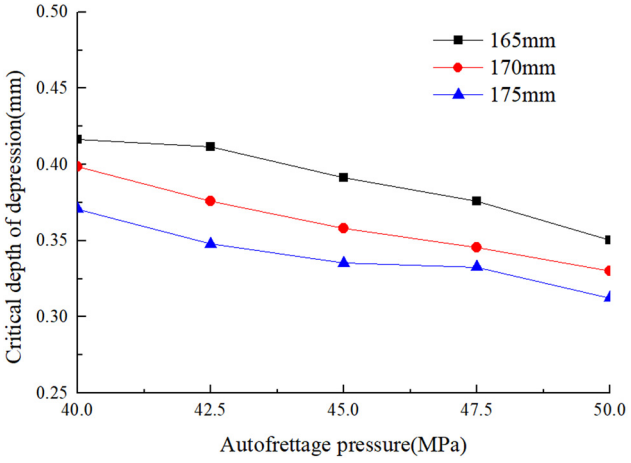

Figure 9: Relationship between the critical depth of depression and autofrettage pressure considering the variation of liner radius.

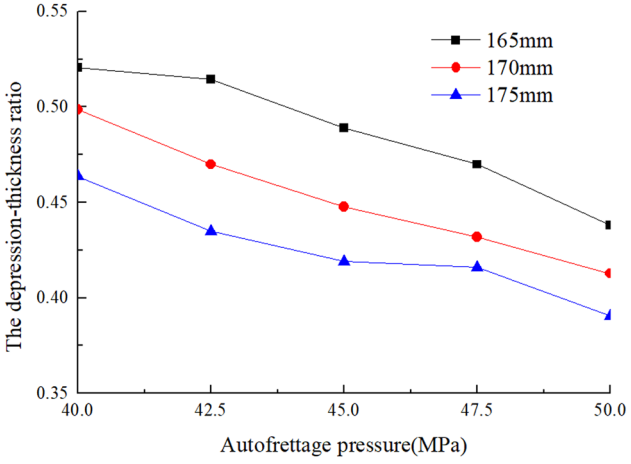

Figure 10: Relationship between the depression-thickness ratio and autofrettage pressure considering the variation of liner radius.

corresponding to the thickness inner liner of 0.8 and 0.7 mm. As the autofrettage pressure increases, local buckling will occur in the metal liner regardless of the thickness. The thinner the inner liner, the smaller the critical depth of the depression, which means that the inner liner is more prone to local buckling and is more sensitive to the size of initial depression after autofrettage.

Table 4: Parameter table for orthogonal case

Case number	Level (autofrettage pressure) (MPa)	Level (liner radius) (mm)	Level (liner thickness) (mm)	Level (length of the straight section) (mm)
1	1(40.0)	1(160.0)	1(0.6)	1(150.0)
2	1(40.0)	2(170.0)	2(0.7)	2(200.0)
3	1(40.0)	3(180.0)	3(0.8)	3(250.0)
4	1(40.0)	4(190.0)	4(0.9)	4(300.0)
5	2(45.0)	1(160.0)	2(0.7)	3(250.0)
6	2(45.0)	2(170.0)	1(0.6)	4(300.0)
7	2(45.0)	3(180.0)	4(0.9)	1(150.0)
8	2(45.0)	4(190.0)	3(0.8)	2(200.0)
9	3(50.0)	1(160.0)	3(0.8)	4(300.0)
10	3(50.0)	2(170.0)	4(0.9)	3(250.0)
11	3(50.0)	3(180.0)	1(0.6)	2(200.0)
12	3(50.0)	4(190.0)	2(0.7)	1(150.0)
13	4(55.0)	1(160.0)	4(0.9)	2(200.0)
14	4(55.0)	2(170.0)	3(0.8)	1(150.0)
15	4(55.0)	3(180.0)	2(0.7)	4(300.0)
16	4(55.0)	4(190.0)	1(0.6)	3(250.0)

4.2.2 Relationship between the critical depth of depression and radius of the inner liner

Keeping the thickness of the liner at 0.8 mm, the radii of the liner are 165, 170, and 175 mm, respectively. The relationship between the critical depth of the depression and the autofrettage pressure is shown in Figure 9 and that between the depression-to-thickness ratio and the autofrettage pressure is shown in Figure 10.

It can be seen from Figures 9 and 10 that, regardless of the diameter, increasing the autofrettage pressure can lead to local buckling of the metal lining. As the radius of the liner increases, both the critical depth and the

Table 3: Table of factor level

Level	Factor			
	Autofrettage pressure (MPa)	Liner radius (mm)	Liner thickness (mm)	Length of the straight section (mm)
1	40	160	0.6	150
2	45	170	0.7	200
3	50	180	0.8	250
4	55	190	0.9	300

Table 5: Analysis of variance

Influencing factor	Autofrettage pressure	Liner radius	Liner thickness	Length of the straight section
Sum of squared deviations of a factor	0.002877	0.017081	0.0833	0.02141
Sum of squared deviation errors			0.000177	
Freedom of each factor	3	3	3	3
Factor-based statistics	16.22	96.27	469.51	120.67

Table 6: Analysis of variance table

Influencing factor	Autofrettage pressure	Liner radius	Liner thickness	Length of the straight section
Sum of squared deviations of a factor	0.004854	0.032071	0.024679	0.035591
Sum of squared deviation errors			0.00029	
Freedom of each factor	3	3	3	3
Factor-based statistics	16.72	110.51	85.04	122.64

depression-to-thickness ratio decrease under the same autofrettage pressure, indicating that the larger the inner liner radius, the easier the local buckling of the liner to occur after autofrettage, and is more sensitive to the size of the initial depression.

4.3 Parametric sensitivity analysis

In order to quantitatively study the influence of the autofrettage pressure, vessel surface area, liner thickness, and the local buckling of cylindrical COPV with initial depression, and the sensitivity analysis of the above four factors, it is necessary to conduct the sensitivity analysis of the four factors above.

4.3.1 Orthogonal case design

Orthogonal experimental design is an efficient design method to study multiple factors and multiple levels. Based on orthogonality, some representative points from the overall points are selected for testing. These representative points have the characteristics of "evenly dispersed, neat, and comparable," which not only reduces the number of necessary sample points but also comprehensively analyzes the sensitivity of each factor [44–46]. Therefore, the orthogonal test is adopted in this article to analyze the orthogonal calculation examples and sort out the most sensitive factors that affect the buckling of the pressure vessel [47]. The design factor levels are shown in Table 3.

According to the feature of the orthogonal test table [40], the parameters for the orthogonal case are shown in Table 4.

4.3.2 Parametric sensitivity analysis

The critical depth of the depression is analyzed according to the numerical example shown in Table 4, and the variance analysis is performed for the critical depth of the depression to judge the influence of the autofrettage pressure, the radius of vessels, thickness of liners, and the straight length on the critical depth of the depression. The results are shown in Table 5.

The variance of each factor is compared. It is found that the influence of four factors on the critical depth of the depressions, from large to small, is as follows: the thickness of the liner, the length of the straight section, the radius of liners, and the autofrettage pressure.

The variance analysis of the depression-to-thickness ratio is carried out to determine the influence of the autofrettage pressure, the radius of the vessel, the thickness of liners, and the length of the straight section on the depression-to-thickness ratio. The results are in Table 6.

The variance of each factor is compared by the analysis of variance. It is found that the influence of the four factors on the depression-thickness ratio, from large to small, is as follows: the length of the straight section, the radius of the liners, the thickness of the liners, and the autofrettage pressure.

5 Conclusions

(1) The numerical and analytical method proposed in this article is an effective strategy to analyze the metal liner buckling behavior of the cylindrical COPV with depression. By comparison with the results in ref. [31], the proposed method can predict the effect of the initial depression size on the local buckling of the metal liner accurately.
(2) For the constant initial depression depth, the inner liner of the pressure vessel is more likely to buckle locally near the depression after autofrettage when the autofrettage pressure is greater. Therefore, a suitable autofrettage pressure should be set to ensure the COPV have a satisfying autofrettage effect and will not enter local buckling.
(3) In the local buckling of the metal liner in the cylindrical composite pressure vessel, the thickness of the metal liner is the most sensitive factor, followed by the length of the straight section and the radius of the liner, while the autofrettage pressure is the least sensitive factor.

The method established in this article can provide references for the engineering design and autofrettage processing of COPV.

Conflict of interest: Authors state no conflict of interest.

References

[1] Holmes GA, Peterson RC, Hunston DL, McDonough WG. E-Glass/DGEBA/m-PDA single fiber composites: the effect of strain rate on interfacial shear strength measurements. Polym Compos. 2010;21(3):450–65.
[2] Sjögren BA, Berglund LA. Toughening mechanisms in rubber-modified glass fiber/unsaturated polyester composites. Polym Compos. 1999;20(5):705–12.
[3] Lei Z, Wang J, Li S. Influence of fiber slippage coefficient distributions on the geometry and performance of composite pressure vessels. Polym Compos. 2016;37(1):315–21.
[4] Hwang TK, Kim HG. Experimental and analytical approach for the size effect on the fiber strength of CFRP. Polym Compos. 2013;34(4):598–606.
[5] Verjenko VE, Adali S, Tabakov PY. Stress distribution in continuously heterogeneous thick laminated pressure vessels. Composite Struct. 2001;54(2/3):371–7.
[6] Krikanov AA. Composite pressure vessels with higher stiffness. Composite Struct. 2000;48(1):119–27.
[7] Bai H, Yang B, Hui H, Yang Y, Yu Q, Zhou Z, et al. Experimental and numerical investigation of the strain response of the filament wound pressure vessels subjected to pressurization test. Polym Compos. 2019;40(5):4427–41.
[8] Erkal S, Sayman O, Benli S, Dogan T, Cinar Yeni E. Fatigue damage in composite cylinders. Polym Compos. 2010;31(4):707–13.
[9] Cohen D, Mantell SC, Zhao L. The effect of fiber volume fraction on filament wound composite pressure vessel strength. Compos Part B: Eng. 2001;32(5):413–29.
[10] Madhavi M, Rao KVJ, Rao KN. Design and analysis of filament wound composite pressure vessel with integrated-end domes. Def Sci J. 2009;59(1):2289–97.
[11] Liu PF, Chu JK, Hou SJ, Xu P, Zheng JY. Numerical simulation and optimal design for composite high-pressure hydrogen storage vessel: a review. Renew Sust Energ Rev. 2012;16(4):1817–27.
[12] CEN International Standard ISO11119 2 Gas Cylinders of Composite Construction specification and Test Methods part2: Fully Wrapped Fiber Reinforced Composite Gas Cylinders with Load sharing Metal Liners. Switzerland: ISO, 2002.
[13] Chen A. Elasto-plastic analysis of residual stress in autofrettage sphere vessel. Chin J Appl Mech. 2008;25(3):512–6.
[14] Lin S, Jia Z, Li W, Li S, Li X, Jia X. Performance study and finite element analysis of autofrettage pressure of thin-walled metal-lined composite gas cylinders. Composite Sci Eng. 2020;312(1):23–8.
[15] Chen HW, Sun HK, Liu TC. Autofrettage analysis of a fibre-reinforced composite tube structure incorporated with a SMA. Composite Struct. 2009;89(4):497–508.
[16] Jahromi BH, Farrahi GH, Maleki M, Nayeb-Hashemi H, Vaziri A. Residual stresses in autofrettaged vessel made of functionally graded material. Eng Struct. 2009;31(12):2930–5.
[17] Lee HJ, Lee JJ, Huh JS. A simulation study on the thermal buckling behavior of laminated composite shells with embedded shape memory alloy (SMA) wires. Composite Struct. 1999;47(1–4):463–9.
[18] Xia M, Takayanagi H, Kemmochi K. Analysis of multi-layered filament-wound composite pipes under internal pressure. Composite Struct. 2001;53(4):483–91.
[19] Jahromi BH, Ajdari A, Nayeb-Hashemi H, Vaziri A. Autofrettage of layered and functionally graded metal–ceramic composite vessels. Composite Struct. 2010;92(8):1813–22.
[20] Kobayashi S. Effect of autofrettage on durability of CFRP composite cylinders subjected to out-of-plane loading. Compos Part B. 2012;43(4):1720–6.
[21] Parker AP. A re-autofrettage procedure for mitigation of Bauschinger effect in thick cylinders. J Press Vessel Technol. 2004;126(4):26–32.
[22] Sun Z, Ren M, Chen H. An engineering algorithm of autofrettage technique for composite overwrapped pressure vessels with metal inner. Acta Materiae Compositae Sin. 2011;28(2):217–21.
[23] Wang Z, Zhao J. Stress Analyses of CFRP cylinder under autofrettage process. Aerosp Mater & Technol. 2017;47(6):29–35.
[24] Moon CJ, Kim IH, Choi BH, Kweon JH, Choi JH. Buckling of filament-wound composite cylinders subjected to hydrostatic pressure for underwater vehicle applications. Composite Struct. 2010;92(9):2241–51.

[25] Aggarwal SC, Cooper MJ. External pressure testing of Insituform lining. Coventry (Lanchester) Polytechnic, Internal Report. Coventry, UK: 1984.
[26] Yang FQ, Zhang TP, Liu ZD, Wang XY. Finite element modeling and buckling analysis of COPV. Vac Cryogenics. 2005;11(1):40–5.
[27] Fu M, Lin S, Chen L, Zhou W. Liner buckling analysis of composite overwrapped pressure vessel. Mater Sci Technol. 2015;23(2):86–90.
[28] Liang C. Numerical simulation of autofrettage and fatigue of filament wound pressure vessel. Aerosp Mater Technol. 2012;42(4):16–20.
[29] Hu ZH, Liu HJ, Wang RG, He XD, Ma L. The study on buckling deformation of composite pressure vessel based on acoustic emission signals. Adv Mater Res. 2009;87–88:445–50.
[30] Saulsberry RL. Private communication of results from experiments at NASA JSC White Sands Test Facility; 2007.
[31] Phoenix S, Kezirian M. Analysis of potential Ti-liner buckling after proof in Kevlar/Epoxy COPV. AIAA/ASME/ASCE/AHS/ASC Structures, Structural Dynamics, & Materials Conference; 2006.
[32] Zhou W, Li C, Ma B, Najafi M. Buckling Strength of a Thin-Wall Stainless Steel Liner Used to Rehabilitate Water Supply Pipelines. J Pipeline Syst Eng Pract. 2016;7(1):4015017.
[33] Lo H, Bogdanoff JL, Goldberg JE, Crawford R. A buckling problem of a circular ring. In: Proceedings of the Fourth US National Congress of Applied Mechanics. 1962. p. 691–5.
[34] Sun C, Shaw WJD, Vinogradov AM. One-way buckling of circular rings confined within a rigid boundary. J Press Vessel Technol. 1995;117(2):162–9.
[35] Yamamoto Y, Matsubara N. Buckling strength of metal lining of a cylindrical pressure vessel. Bull JSME. 1969;12(51):421–9.
[36] Yamamoto Y, Matsubara N. Buckling strength of steel cylindrical liners for waterway tunnels. Theor Appl Mech. 1981;30:225–35.
[37] Wang R, Xiaodong HE, Zhaohui HU, Liu W, Shi J. Structure analysis of composite pressure vessel with ultra-thin metallic liner. Acta Materiae Compositae Sin. 2010;27(4):131–8.
[38] Vasilikis D, Karamanos SA. Stability of confined thin-walled steel cylinders under external pressure. Int J Mech Sci. 2009;51(1):21–32.
[39] Daniel V, Karamanos SA. Buckling design of confined steel cylinders under external pressure. J Press Vessel Technol. 2011;133(1):011205.
[40] Nayak GC, Zienkiewicz OC. Elasto-plastic stress analysis. A generalization for various contitutive relations including strain softening. Int J Numer Meth Eng. 2010;5(1):113–35.
[41] De Lorenzis L, Wriggers P, Hughes TJR. Isogeometric contact: a review. GAMM-Mitteilungen. 2014;37(1):85–123.
[42] Reddy JN. Theory and analysis of elastic plates and shells. J Am Chem Soc. 1999;99(2):633–4 (Second edn.).
[43] Brush DO, Almroth BO, Hutchinson JW. Buckling of bars, plates, and shells. J Appl Mech. 1975;42(4):911.
[44] Cao WH, Liu HB, Li XF. Optimization analysis of the injection molding process based on orthogonal test method and uniform design. Appl Mech Mater. 2013;401–403:863–6.
[45] Zhao C, Chen X, Zhao C. Study on CO_2 capture using dry potassium-based sorbents through orthogonal test method. Int J Greenh Gas Control. 2010;4(4):655–8.
[46] Kang L, Dixon S, Wang K, Dai J. Enhancement of signal amplitude of surface wave EMATs based on 3-D simulation analysis and orthogonal test method. Ndt E Int. 2013;59:11–7.
[47] Liu Z, Zhu R. Key parameters of pressure vessel auto-reinforcement technology and influence on auto-reinforcement technology. Chem Equip Technol. 2020;41(6):20–5.